

Effect of Strain Rate on Modelling Predictions of Hot Tearing During Direct Chill Casting of an Aluminum-Magnesium Alloy Using the Dimensionless Niyama Criterion

Ruifeng Dou^(a), A.B. Phillion^{(b)*}

^(a)School of Mechanical Engineering, University of Science and Technology Beijing, Beijing, 100083 China

^(b)Department of Materials Science and Engineering, McMaster University, Hamilton, ON, L8S 4L7, Canada

*Corresponding author: A.B. Phillion, Email: andre.phillion@mcmaster.ca.

Abstract: Hot tearing is strongly linked with the applied semi-solid strain rate. This defect is commonly qualitatively predicted using a pressure drop equation in the mushy zone that includes the effects of both tensile deformation perpendicular to the thermal gradient and shrinkage feeding. In this study, the effect of strain rate parallel to the thermal gradient is additionally introduced in order to assess its effect on hot tearing predictions. The deformation and shrinkage pore fractions are obtained on the basis of the dimensionless Niyama criterion and a scaling variable method. This Pore Fraction hot tearing model is first applied to the binary Al-Cu system under conditions of directional solidification. It is shown that for the same Niyama criterion, a decrease in the cooling rate increases both the deformation and shrinkage pore fractions because of an increase in the time spent in the brittle temperature region. Then, using a finite element simulation, the pore fraction distributions during Direct Chill casting of the AA5182 aluminum alloy are obtained. It is shown that including the strain rate parallel to the thermal gradient significantly improved the predictive quality of hot tearing criteria based on the pressure drop equation. Further, an increase in the casting speed increases the deformation and shrinkage pore fractions and causes the maximum point of pore fraction to move towards the base of the casting.

Keywords: DC casting, Niyama criterion, Pore fraction, Hot tearing.

1 Introduction

The direct-chill (DC) casting process often involves defects such as hot tearing,^[1, 2] cold cracks,^[3, 4, 5] butt curl,^[6] macro/micro segregation,^[7, 8] and shrinkage porosity.^[9] Hot tearing and shrinkage porosity in particular have been widely recognized in the literature for more than 10 decades. Shrinkage porosity is caused by the volume change occurring during solidification combined with the restricted feeding of liquid to the final solidifying region. Hot tearing is a defect with similar formation mechanisms, but also requires tensile deformation of the mushy zone^[10]. Hot tearing and porosity are known to be inter-related. For example, it has been shown that hot tears nucleate on small intergranular pores^[11], and that a reduction in porosity significantly increases semi-solid ductility^[12].

Several hot tearing criteria have been developed on the basis of different parameters, e.g., strain,^[13] strain rate,^[14, 15] alloy composition and solidification conditions.^[1, 16] The so-called RDG criterion^[15] is a prominent criterion based on the liquid pressure drop in the mushy zone that combines the effects of both tensile deformation perpendicular to the thermal gradient and shrinkage feeding on hot tear formation. The hot tearing predictor is given by the strain rate that satisfies the critical pressure drop ΔP_{cr} required for hot tear formation. Although this criterion has achieved much recognition in the literature, it cannot distinguish between shrinkage porosity and hot tearing, especially for low thermal gradients.^[17]

The Niyama criterion, Ny , is commonly-used as a qualitative predictor of solidification shrinkage porosity during metal casting processes^[18]. Recently, Carlson and Beckermann^[9] proposed a dimensionless form of the Niyama criterion, Ny^* , that directly predicts shrinkage pore fractions. As with the RDG criterion, Ny^* was developed based on the liquid pressure drop in the mushy zone, but however it neglects tensile deformation. Within the framework of Ny^* , ΔP_{cr} marks the point at which liquid flow ceases in the mushy

zone. Thus, any solidification occurring after liquid feeding has ceased can result in shrinkage porosity. Monroe and Beckermann^[17] later modified Ny^* by adding a term related to strain rate perpendicular to the thermal gradient into the pressure drop equation. With the same method, *i.e.* tracking of solidification and deformation after liquid feeding cessation, both the shrinkage and deformation pore fractions were predicted. The deformation pore fraction is critical for hot tearing because this defect is related to mushy zone stresses and strains.^[10] The main difference between the RDG criterion and the work of Monroe and Beckerman is that while the former predicts a strain rate satisfying ΔP_{cr} , the latter predicts the evolution of deformation-related porosity after ΔP_{cr} is reached based on an given strain rate.

In this study, a Pore Fraction hot tearing model for predicting the evolution of pore fraction during solidification is presented that follows the method developed by Monroe and Beckermann^[17] but additionally considers the effects of deformation parallel with the thermal gradient in the mushy zone. This model is then applied to the DC casting of an Al-Mg alloy, AA5182. The effect of casting speed on hot tear formation is investigated.

2 Model Development

2.1 Pore Fraction hot tearing model

The Niyama criterion^[18] is defined as,

$$Ny = \frac{G}{\sqrt{\dot{T}}} \quad (1)$$

where G is the temperature gradient and \dot{T} is the cooling rate having a positive value if the temperature is decreasing. This criterion is evaluated at a temperature near the end of solidification, when solidification shrinkage forms.

The dimensionless Niyama criterion^[9] is a modified form of Eq. [1] that allows for prediction of pore fractions during casting,

$$Ny^* = \sqrt{\frac{\Delta P_{cr} \lambda_2^2}{\beta \mu \Delta T_f}} \frac{G}{\sqrt{\dot{T}}} \quad (2)$$

where ΔP_{cr} corresponds to the critical pressure drop, λ_2 is the secondary dendrite arm spacing (SDAS), β is the solidification shrinkage, μ is the viscosity, and $\Delta T_f = T_{liq} - T_{sol}$ is the solidification interval where T_{liq} is the liquidus temperature and T_{sol} is the temperature at which the alloy is fully solidified.

The governing equations for Ny^* is conservation of mass using a control volume consisting of dendrite arms and interdendritic liquid^[15] and Darcy's Law governing pressure drop in the mushy zone,

$$\text{div} < \rho V > - V_T \frac{\partial < \rho >}{\partial x} = 0 \quad (3)$$

$$f_l V_{lx} = - \frac{K}{\mu} \frac{dp}{dx} \quad (4)$$

where the notation $< \cdot >$ is employed to indicate values that are locally averaged over the liquid and solid phases, ρ represents density, V represents velocity, $V_T = \frac{\dot{T}}{G}$ is the isotherm speed (growth interface velocity), with a direction aligned with that of the temperature gradient, μ is the viscosity, K is the permeability, and P is the melt pressure. Thus, the average specific mass and average mass flow are given by $< \rho > = \rho_s f_s + \rho_l f_l$, and $< \rho V > = \rho_s f_s V_s + \rho_l f_l V_l$, where f_l and f_s are the volume fractions of liquid and solid, f_l is equal to $(1 - f_s)$, and the densities of the two phases, ρ_s and ρ_l , are assumed to be constant but not equal.^[15]

Both Monroe and Beckerman's extension of Ny^* ^[17] and the RDG criterion^[15] were developed from Eqs. [3] and [4] based on the assumptions that: (1) fluid moves only along the thermal gradient and thus equates to a one-dimensional fluid flow, and (2) the solid deforms only in a direction transverse to the fluid motion/thermal gradient. During metal casting, the first assumption is appropriate, since the mushy zone consists of a continuous path between the liquid and solid phases enabling flow in a single direction. However, deformation of solid in a direction parallel to the thermal gradient is also possible in addition to

deformation in the transverse direction. Furthermore, the amount of such deformation can be easily calculated using finite element models of casting processes (e.g. [13, 19, 20]).

Including the solid deformation in a direction parallel to the thermal gradient will not make the derivation of the pressure drop equation any more complex as compared previous work. From Eq. [3], mass conservation can be presented considering solid deformation in directions both parallel and perpendicular to the thermal gradient. First, under the given assumptions, Eq. [3] can be expanded,

$$\frac{\partial(\rho_l f_l V_{lx})}{\partial x} + \frac{\partial(\rho_s f_s V_{sx})}{\partial x} + \frac{\partial(\rho_s f_s V_{sy})}{\partial y} = V_T \left[\frac{\partial(\rho_s f_s)}{\partial x} + \frac{\partial(\rho_l f_l)}{\partial x} \right] \quad (5)$$

where V_{sx} and V_{sy} are the relevant solid deformation velocities as shown in Fig. 1. Second, assuming that f_s and f_l only change over x (along the thermal gradient), Eq. [5] can be rewritten as,

$$\frac{\partial(f_l V_{lx})}{\partial x} + (1 + \beta) \left[V_{sx} \frac{df_s}{dx} + f_s \dot{\epsilon}_{px} + f_s \dot{\epsilon}_{py} \right] = V_T \beta \frac{\partial f_s}{\partial x} \quad (6)$$

where $\dot{\epsilon}_{px} = \frac{\partial V_{sx}}{\partial x}$ and $\dot{\epsilon}_{py} = \frac{\partial V_{sy}}{\partial y}$ are the strain rates parallel with and perpendicular to the thermal gradient.

Third, employing the same method as used by Rappaz et al.^[15], Eq. [6] can be integrated over x , giving,

$$f_l V_{lx} + (1 + \beta) \left[V_{sx} f_s + \int f_s (\dot{\epsilon}_{px} + \dot{\epsilon}_{py}) dx \right] - V_T \beta f_s = C = -V_T \beta \quad (7)$$

where the constant of integration, C , has been replaced by the boundary condition, $C = -V_T \beta$. This equation predicts the liquid velocity at any position in the mushy zone. Finally, Darcy's law is used to link liquid melt pressure and velocity. Replacing the $f_l V_{lx}$ term of Eq. [7] with Eq. [4] and then integrating from $x_{f_l=1}$ to $x_{f_l=f_{lcr}}$ gives a modified form of the pressure drop equation,

$$\Delta P_{cr} = (1 + \beta) \mu \int_{x_{f_l=f_{lcr}}}^{x_{f_l=1}} \frac{1}{K} \left[V_{sx} f_s + \int f_s (\dot{\epsilon}_{px} + \dot{\epsilon}_{py}) dx \right] dx + V_T \beta \mu \int_{x_{f_l=f_{lcr}}}^{x_{f_l=1}} \frac{f_l}{K} dx \quad (8)$$

assuming that μ and V_T are constant throughout the mushy zone. Further, $V_T = \frac{\dot{T}}{G}$ is evaluated at a critical temperature near the solidus as defined for Ny . In this equation, ΔP_{cr} corresponds to the critical pressure drop between $f_l=1.0$ and a critical liquid fraction where feeding has ceased, f_{lcr} .

Since the temperature gradient, cooling rate, and strain rate are assumed constant, the integration variable of Eq. [8] can be changed from position to fraction liquid and the strain rate terms can be taken out of the integral, yielding,

$$\Delta P_{cr} = \frac{(1+\beta)\mu}{G} \int_{f_{lcr}}^1 \frac{1}{K} \left[V_{sx} f_s + \frac{(\dot{\epsilon}_{px} + \dot{\epsilon}_{py})}{G} \int_0^{f_{lcr}} (1-f_l) \frac{dT}{df_l} df_l \right] \frac{dT}{df_l} df_l + \frac{\dot{T}\beta\mu}{G^2} \int_{f_{lcr}}^1 \frac{f_l}{K} \frac{dT}{df_l} df_l. \quad (9)$$

If the strain rates ($\dot{\epsilon}_{px}$ and $\dot{\epsilon}_{py}$ are set to zero, Eq. [9] is identical with the result of Carlson and Beckerman^[9] in deriving Ny^* since the term $V_{sx} f_s = 0$ (recall that $\dot{\epsilon}_{px} = \frac{\partial V_{sx}}{\partial x}$ by definition), and can be used for predicting shrinkage porosity. If only $\dot{\epsilon}_{px}$ is set to zero, Eq. [12] matches the RDG criterion^[15]

Introducing a dimensionless temp. $\theta = (T - T_{sol})/\Delta T_f$ where ΔT_f is the freezing range of the alloy, and rearranging Eq. [9] yields

$$\begin{aligned} \Delta P_{cr} &= \frac{(1 + \beta) \mu \Delta T_f^2 (\dot{\epsilon}_{px} + \dot{\epsilon}_{py})}{G^2} I_{de} + \frac{(1 + \beta) \mu \Delta T_f \dot{\epsilon}_{px} \lambda_2}{G} I_{sh\dot{\epsilon}} + \frac{\dot{T} \beta \mu \Delta T_f}{G^2} I_{sh}, \\ &= \frac{(1+\beta) \mu \Delta T_f^2 (\dot{\epsilon}_{px} + \dot{\epsilon}_{py})}{G^2} I_{de} + \frac{(1+\beta) \mu \Delta T_f V_{sx}}{G} I_{sh\dot{\epsilon}} + \frac{\beta \mu \Delta T_f V_T}{G} I_{sh}, \end{aligned} \quad (10a)$$

$$I_{de} = \int_{f_{lcr}}^1 \left[\frac{1}{K} \int_0^{f_{lcr}} (1-f_l) \frac{d\theta}{df_l} df_l \right] \frac{d\theta}{df_l} df_l \quad (10b)$$

$$I_{sh\dot{\epsilon}} = \int_{f_{lcr}}^1 \frac{1-f_l}{K} \frac{d\theta}{df_l} df_l \quad (10c)$$

$$I_{sh} = \int_{f_{lcr}}^1 \frac{f_l}{K} \frac{d\theta}{df_l} df_l \quad (10d)$$

In this expression, I_{de} is associated with the term related to the deformation, I_{sh} is associated with the term related to the shrinkage, and $I_{sh\dot{\epsilon}}$ is associated with the term related to the deformation-induced shrinkage. As can be seen, the second and third terms of Eq. [10a] have the same form, related through the isotherm velocity V_T and solid deformation velocity V_{sx} . The permeability K has also been left inside the integrations of I_{de} , $I_{sh\dot{\epsilon}}$, and I_{sh} because many different empirical relations exist for this function,^[21, 22] such as the Kozeny–Carman relation.^[21]

Following Monroe and Beckerman^[17], it is assumed that fluid flow ceases once the pressure drop exceeds ΔP_{cr} . Thus, for a given value of ΔP_{cr} , the critical fraction of fluid f_{lcr} can be obtained from Eq. [10]. Further shrinkage and deformation beyond f_{lcr} will result in the formation of porosity.

When flow stops at f_{lcr} , mass conservation can be applied to determine the porosity that must form to feed the remaining shrinkage^[17],

$$f_{p,sh} = \frac{\beta}{1+\beta} f_{lcr} \quad (11)$$

A similar set of variables can be used to calculate deformation-related porosity, $f_{p,de,ex}$ and $f_{p,de,ey}$,

$$f_{p,de,ex} = \frac{\dot{\epsilon}_{px}\Delta T_f}{\dot{T}} \int_0^{f_{lcr}} (1-f_l) \frac{d\theta}{df_l} df_l \quad (12)$$

$$f_{p,de,ey} = \frac{\dot{\epsilon}_{py}\Delta T_f}{\dot{T}} \int_0^{f_{lcr}} (1-f_l) \frac{d\theta}{df_l} df_l \quad (13)$$

Finally, because of the term $I_{sh\dot{\epsilon}}$ in Eq. [10], there is additionally strain rate-induced shrinkage porosity,

$$f_{p,sh\dot{\epsilon}} = \frac{G\dot{\epsilon}_{px}\lambda_2}{\dot{T}} (1-f_l) = \frac{V_{sx}}{V_T} (1-f_{lcr}) \quad (14)$$

Thus, as shown in Eqs. [11]–[14], the total porosity that forms during the late stages of solidification below f_{lcr} consists of four components: $f_{p,sh}$, $f_{p,de,ex}$, $f_{p,de,ey}$, and $f_{p,sh\dot{\epsilon}}$. Further, the total deformation pore fraction and total pore fraction can be computed, and are denoted as $f_{p,de}$ and $f_{p,sum}$, i.e.,

$$f_{p,de} = f_{p,de,ex} + f_{p,de,ey} \quad (15)$$

$$f_{p,sum} = f_{p,sh} + f_{p,sh\dot{\epsilon}} + f_{p,de,ex} + f_{p,de,ey} \quad (16)$$

Since only a positive strain rate increases pore fraction to result in the formation of a hot tear, the occurrence of a negative strain rate is ignored in the following analysis.

2.2 Effect of strain rate parallel with thermal gradient on pore fraction

To investigate the predictions of the Pore Fraction hot tearing model, and verify its accuracy, the present results are compared against the results provided by Monroe^[17] for Al-Cu alloys using the same solid fraction–temperature curve and input parameters given in their work (Eq. [17] and Table I in [17]). Most importantly, ΔP_{cr} is set to 1.0 atm. Note also that the eutectic temperature in [17] should have been given as 821 K (547.85 °C) and not 855 K (581.85 °C) to match the Al-Cu binary phase diagram. To additionally examine the effect of the strain rate parallel with the thermal gradient, $\dot{\epsilon}_{px}$ is arbitrarily assigned a value of 0.1 times $\dot{\epsilon}_{py}$. Fig. 2 shows the pore fraction curves as function of Ny^* for an Al-3wt.%Cu alloy. The results given in Fig. 2 match Fig. 3 in [17] but with the addition of the curves $f_{p,de,ex}$ (Eq. [12]) and $f_{p,sh\dot{\epsilon}}$ (Eq. [14]). As can be seen, the curves for $f_{p,sh}$, and $f_{p,de,ey}$ predict significant porosity, especially at lower values of Ny^* . For the same Ny^* , the value of $f_{p,de,ex}$ is 0.1 times that of $f_{p,de,ey}$, as expected. Clearly, the positive value of $\dot{\epsilon}_{px}$ increases the total deformation pore fraction $f_{p,de}$, and $\dot{\epsilon}_{px}$ has the same impact on the deformation pore fraction as $\dot{\epsilon}_{py}$ has. The value of $f_{p,sh\dot{\epsilon}}$ has a magnitude of 10^{-7} , which is negligible compared with the values of $f_{p,sh}$, $f_{p,de,ey}$, and $f_{p,de,ex}$.

The effect of alloy composition C_0 , thermal gradient G , and cooling rate \dot{T} on the pore fraction is shown in Fig. 3. The red and black curves in Fig. 3 are both calculated with a Niyama criterion (Eq. [1]) value of 100, with the black curves matching those from Fig. 5 in [17]. The $f_{p,de,ex}$ curve has the same trend as the $f_{p,de,ey}$ curve, increasing with composition up to $C_0 = 0.25$ ^[17] and then decreasing at higher alloy concentrations, identifying the point of maximum hot tearing susceptibility. Thus, the strain rates parallel with and perpendicular to the thermal gradient have the same effect on pore development. As the value of $f_{p,sh\dot{\epsilon}}$ was negligible, it is not shown in Fig. 3. Note that experimentally (e.g. [23]), the maximum hot tearing susceptibility for Al-Cu alloys is found at ~Al-1wt%Cu alloys and not Al-0.25wt.%Cu. As explained in detail in [17], $C_{0,max}$ corresponds to the maximum solidification interval, and it is strongly related to the fraction liquid for grain bridging. In this work, it has been assumed that grain bridging occurs at $f_l=0$ in order to compare the results in the present manuscript against [17]. An increase in $f_{l,gb}$ to the usual value of 0.02 ($f_s=0.98$) will increase $C_{0,max}$ as well, to 1.32wt.%Cu.

Surprisingly, by comparing the red and black curves, it can be seen that even with the same Niyama criterion, the pore fractions differ for different cooling rates and thermal gradients. Given the same Niyama criterion, the application of a low cooling rate results in a high pore fraction and thus a high propensity for hot tearing because this results in a decrease in the isotherm speed V_T (Eq. [3]), which in turn increases the solidification time and finally increases the duration within the brittle temperature region (BTR, *i.e.* the temperature region within the semi-solid where the ductility of the alloy is virtually zero^[24] [25, 26]). The effect is much more significant on the deformation-related porosity ($f_{p,de,ey}$ curve) as compared to the shrinkage-related porosity ($f_{p,sh}$ curve). This is because the deformation-related porosity is both directly proportional to f_{lcr} and inversely proportional to \dot{T} whereas the shrinkage-related porosity is only proportional to f_{lcr} . Thus, the Niyama criterion is not sufficient to predict hot tearing susceptibility. Furthermore, although the red and black curves for $f_{p,sh}$ are similar, identical Niyama values do not indicate identical levels of shrinkage porosity in the context of the present model.

3 Pore fraction prediction for DC casting under different conditions

In combination with a finite element simulation, the Pore Fraction hot tearing model can be applied to analyze the distribution of $f_{p,de}$ during DC casting of AA5182 aluminum alloy cylindrical billets.

3.1 Coupled thermal-mechanical DC casting model

The DC casting process of an AA5182 round billet was simulated using an axisymmetric coupled thermomechanical model implemented in the commercial FE code Abaqus, which is schematically shown in Fig. 4. The details of the simulation methodology, boundary conditions, and constitutive behaviour are provided in Jamaly et al.^[13]. The key feature for predicting hot tearing using the Pore Fraction hot tearing model is the alloy's constitutive behaviour since this controls the development of the strain rate tensor within the mushy zone. As reported in [13], the modified Ludwik equation developed by Alankar and Wells^[27] is used to simulate the constitutive behavior of the alloy at temperatures below the solidus temperature, while the constitutive behaviour between the solidus temperature (796.15 K (523 °C)) and the temperature for mechanical coalescence (875.15 K (602 °C)) is simulated based on microstructure and fraction solid according to a model proposed by Phillion et al.^[28] Above the temperature for mechanical coalescence, a low constant yield strength is specified, matching the yield strength values calculated with the model proposed by Phillion et al.^[28] at the temperature for mechanical coalescence.

3.2 Implementation of pore prediction model

The pore fractions were calculated using a C# purpose-written code. First, the DC casting finite element simulation of Jamaly et al. [13] was run to completion. Second, the cooling rate, thermal gradient, and strain rate was extracted from the simulation output at the critical temperature of 819.15 K (546 °C), corresponding to a solid fraction of 0.98. Third, all the negative strain rate values were set to zero because they do not

increase the pore fraction. Finally, the Pore Fraction hot tearing model was applied to calculate $f_{p,sh}$, $f_{p,de,\varepsilon y}$, $f_{p,de,\varepsilon x}$, and $f_{p,sh\varepsilon}$.

The computation of permeability via the Kozeny–Carman equation requires the secondary dendrite arm spacing λ_2 (SDAS). Following Glenn et al.^[29], SDAS is calculated as

$$\ln(\lambda_2) = 0.47 \ln(\tau_f) + 1.75 \quad (17)$$

where the unit of λ_2 is μm and τ_f is the local solidification time (s) defined as the duration between the liquidus (910.15 K (637°C)) and solidus (796.15 K (523°C)) temperatures.

The computation of the strain rates parallel with and perpendicular to the fluid flow within the mushy zone requires a rotation of the strain rate tensor from the global axi-symmetric coordinate system to the local system aligned with the thermal gradient. The strain rate is calculated as follows,

$$A = R \times \dot{\varepsilon}_{ij} \times R', \quad (18a)$$

$$R = \begin{bmatrix} \cos\left(\frac{\pi}{2} - \gamma\right) & \sin\left(\frac{\pi}{2} - \gamma\right) \\ -\sin\left(\frac{\pi}{2} - \gamma\right) & \cos\left(\frac{\pi}{2} - \gamma\right) \end{bmatrix}, \quad (18b)$$

where γ is the rotation angle between the radius and the thermal gradient, R is the transformation matrix, $\dot{\varepsilon}_{ij}$ is the strain rate tensor in the global coordinates, and A is the strain rate in the local coordinates. The strain rate perpendicular to the thermal gradient, $\dot{\varepsilon}_{py}$, is given by $A_{11} + \dot{\varepsilon}_{pH}$ where $\dot{\varepsilon}_{pH}$ is hoop plastic strain rate, and the strain rate parallel to the thermal gradient, $\dot{\varepsilon}_{px}$, is A_{22} .

3.3 Effect of strain rate parallel with thermal gradient on pore fraction

Fig. 5 shows (a) the pore fraction distribution along the centerline of the billet at a casting speed of $56 \text{ mm} \cdot \text{min}^{-1}$, and (b) the corresponding strain rates parallel with and perpendicular to the thermal gradient. Fig. 5(a) shows that the part of the billet at 16 mm from the bottom of the billet has the highest pore fractions $f_{p,de}$ and $f_{p,sum}$, which make this region prone to hot tearing. The total deformation pore fraction $f_{p,de}$ then undergoes a steep decrease as the height increases from 16 mm, and $f_{p,de}$ is less than 10^{-4} at 48 mm from the bottom of the billet. After a distance of 96 mm from the bottom of the billet, $f_{p,de}$ starts to increase again as the strain rate $\dot{\varepsilon}_{py}$ acquires a tensile nature (as shown in Fig. 5(b)) and finally reaches a plateau. Note that each height value is a multiple of four since that is the mesh size in the finite element simulation. Although the maximum value of $\dot{\varepsilon}_{py}$ is similar to the maximum value of $\dot{\varepsilon}_{px}$, the pore fraction in the steady state regime above 96 mm is significantly smaller than that at 16 mm because of the different thermal conditions. In the start-up regime, the cooling rate and thermal gradient are very low (although the Niyama value is larger than the steady state) because the contact heat transfer coefficient between the billet and the bottom block is considerably lower than the water film heat transfer coefficient.

The importance of including the strain rate parallel to the thermal gradient is evident in Fig. 5(b), since all of the tensile deformation occurring in the start-up region is in this direction, while $\dot{\varepsilon}_{py}$ remains at zero until a distance of 96 mm from the bottom of the billet. Without including $\dot{\varepsilon}_{px}$, the deformation pore fraction would be very small within a distance of 96 mm from bottom of the billet, making it appear that the shrinkage pore fraction dominates within this region. This would lead to erroneous conclusions regarding the relative importance of the shrinkage and deformation pore fractions as predictors for hot tearing formation within the start-up region of DC casting. Furthermore, this would lead to the appearance that the total pore fraction increases with increasing distance from bottom of the billet, i.e. hot tearing susceptibility is increased in the steady-state region as compared to the start-up region. This would not match industrial experience.

Fig 6. shows the contour plots of the pore fractions $f_{p,de}$, $f_{p,sum}$ and the critical liquid fraction f_{lcr} using the casting conditions corresponding to Fig. 5. The highest values of the pore fractions $f_{p,de}$ and $f_{p,sum}$ appear at a radius of 15 mm and a distance of 16 mm from bottom of the billet. The part at which $f_{p,de}$ exceeds 10^{-2} is concentrated in a small region, between 12 and 26 mm above the bottom block and within 70 mm on the centerline. This region is within the start-up phase of DC casting. Thus, if hot tears are to occur, they should appear within this region. Large values of $f_{p,de}$ equate to a high susceptibility to hot tearing due to their link with tensile strain. Examining Fig. 6(c), it can be seen that the highest f_{lcr} , *i.e.* the fraction of liquid at which feeding ceases to occur, is found much further up the casting, within the steady-state region, and has a value of $f_l = 0.95$. However, the highest f_{lcr} doesn't correspond with the highest $f_{p,de}$ and $f_{p,sum}$ because of the strong dependence of these terms on thermal gradient, cooling rate, and strain rate.

3.4 Effect of casting speed

Fig. 7 shows the effect of casting speed on (a) total pore fraction $f_{p,sum}$ and (b) total deformation pore fraction $f_{p,de}$ along the centerline of the billet. Both figures show the maximum values of pore fraction as well as the hot tearing sensitivity increase with increasing casting speed. Similar results were obtained by Drezet and Rappaz,^[30] that is, in the DC casting process, a high casting speed results in large pressure drops and high hot tearing tendencies according to the RDG criterion. However, Fig. 7 also shows that the location of the maximum point of the pore fraction moves downward along the centerline as the casting speed increases. This phenomenon indicates that a high casting speed equates to a high hot tearing tendency, but hot tearing in this case occurs early after the start of DC casting. Beyond a distance of 50 mm from the bottom of the billet, the deformation pore fraction rapidly increases again in cases in which the casting speeds are 56 and 66 mm·min⁻¹. This condition is due to the increase in the strain rate $\dot{\epsilon}_{py}$, as shown in Fig. 5(b). In contrast, nearly no increase in the deformation pore fraction occurs when the casting speed is 46 mm·min⁻¹.

In the start-up region of the casting, the maximum pore fractions are observed at 24, 16, and 12 mm from the bottom for the casting speeds of 46, 56, and 66 mm·min⁻¹, respectively. Fig. 8 shows the curves of $f_{p,de}$ and $f_{p,sum}$ along the radius and crossing the maximum points at different casting speeds. Similar to the trend shown in Fig. 7, the increase in casting speed raises the pore fraction and finally raises the hot tearing probability. The regions where $f_{p,de}$ exceeds 10^{-3} are mainly within the radius range of 0 mm to 100 mm. Hence, the central part of the billet is sensitive to hot tearing.

3.5 Comparison with Prior Models

Based on RDG criterion, Drezet et al.^[30] concluded that during the DC casting, the bottom of the billet is more sensitive to hot tearing than the region of the primary cooling, and the process conditions used to start the casting are critical. Hao et al.^[31] investigated hot tearing during DC casting of AZ31 magnesium billet, showing that the locations near the base of the ingot are more sensible to hot tearing, and that faster casting speeds tend to exacerbate hot tear formation. Thus, the results given in this work that include a term accounting for the strain rate parallel to the thermal gradient match qualitatively the previous findings. However, as shown in Figure 5, without including the term $\dot{\epsilon}_{px}$, hot tearing susceptibility is predicted to be enhanced in the start-up region because of the shrinkage term and not because of the strain-rate term. Ideally, a criterion for predicting hot tearing would show greater dependence on the amount of deformation as compared to porosity developing within the semi-solid. In work on steels, Monroe and Beckermann^[32] developed a hot tearing indicator in which hot tearing susceptibility was determined based on the integral of the volumetric strain rate after liquid feeding has ceased. In that work shrinkage-based and deformation-based porosity were only loosely coupled whereas in our model the shrinkage and deformation terms are fully integrated. Thus, the Pore Fraction hot tearing model proposed in this work represents the continued

and natural evolution of the RDG criterion towards ultimately quantitatively predicting the occurrence of hot tears.

4 Conclusions

The strain rate parallel with the thermal gradient has been added to a pressure drop equation in the mushy zone that already includes the effects of strain rate perpendicular to the thermal gradient and shrinkage feeding in order to improve hot tearing predictions based on the dimensionless Niyama criterion. Application of this criterion to analytical simulations of the casting of an Al-3wt%Cu alloy, and FE simulations of the DC casting process for the aluminum alloy AA5182 has demonstrated the following:

- (a) For the casting simulation of Al-3wt%Cu alloy, under the same Niyama criterion, a decrease in the cooling rate increases significantly the deformation pore fraction, and increases moderately the shrinkage pore fraction. Thus, the Niyama criterion is insufficient as a predictor for hot tear formation.
- (b) For the DC casting simulation and hot tearing prediction of AA5182 alloy,
 - Including the strain rate parallel to the thermal gradient strongly improves the predictive quality of hot tearing criteria based on a pressure drop equation. Without this term, the deformation pore fraction would be very small in the start-up region of DC casting as compared to the shrinkage pore fraction, and the total pore fraction would be highest in the steady-state region.
 - An increase in casting speed increases both the deformation and shrinkage pore fractions, resulting in an increase in the probability of hot tearing. An increase in casting speed also causes the location of highest hot tearing susceptibility to move towards the bottom part of the billet.

Acknowledgment:

This work was funded by the China Scholarship Council, and the National Science and Engineering Research Council of Canada.

References

- [1] J. Campbell: Castings. 2nd edition, 2003, Oxford, Butterworth-Heinemann.
- [2] J. Drezet, M. Rappaz, Y. Krahenbuhl: *Mater. Sci. Forum*, 1996, vol. 217-222, pp. 305-310.
- [3] D. G. Eskin, M. Lalpoor, L. Katgerman: : published in TMS-Light Metals, S.J. Lindsay, ed., Warrendale, PA, 2011, pp. 669-674.
- [4] B. Commet, P. Delaire, J. Rabenberg, et al.: published in TMS-Light Metals, P.N. Crepeau, ed., Warrendale, PA, 2003, 711-717
- [5] M. Lalpoor, D. G. Eskin, et al.: *Mater. Sci. Eng. A*, 2011, vol. 528, p. 2831-2842.
- [6] J. Grandfeld, P. McGlade: *Mater. Sci. Forum*. 1996, vol. 20, pp. 29-51.
- [7] D.G. Eskin, Q. Du, L. Katgerman: *Metall. Mater. Trans. A*, 2008, vol. 39A, pp. 1206-1212.
- [8] D.G. Eskin, L. Katgerman: *Mater. Techn.*, 2009, vol. 24, pp. 152-156.
- [9] K. D. Carlson, C. Beckermann: *Metall. Mater. Trans. A*, 2009, vol. 40A, pp. 163-175.
- [10] J. A. Dantzig, M. Rappaz: Solidification. 1st edition, 2009, Lausanne, EPFL Press.
- [11] I. Farup, J.M. Drezet, M. Rappaz: *Acta Mater.*, 2001, vol. 49, pp. 1261-1269.
- [12] A.B. Phillion, S.L. Cockcroft, P.D. Lee: *Mater. Sci. Eng. A*, 2008, vol. 491, pp. 237-247.
- [13] N. Jamaly, A. B. Phillion, J. M. Drezet: *Metall. Mater. Trans. B*, 2013, vol. 44B, 1287-1295.
- [14] Y. Won, T. Yeo, D. Seol, et al.: *Metall. Mater. Trans. B*, 2000, vol. 31B, pp. 779-794.
- [15] M. Rappaz, J.-M. Drezet, M. Gremaud: *Metall. Mater. Trans. A*, 1999, vol. 30A, pp. 449-455.
- [16] T. Clyne, G. Davies: *British Foundryman*, 1981, vol. 74, pp. 65-73.
- [17] C. Monroe, C. Beckermann: *JOM*, 2014, vol. 66, pp. 1439-1445.
- [18] E. Niyama, T. Uchida, M. Morikawa, and S. Saito: *AFS Cast Met. Res. J.*, 1982, vol. 7, pp. 52-63.
- [19] J. Sengupta, S.L. Cockcroft, et al.: *Mater. Sci. Eng. A*, 2005, vol. 397, pp. 157-77.
- [20] J.-M. Drezet and M. Rappaz: *Metall. Mater. Trans. A*, 1996, vol. 27A, pp. 3214-25.
- [21] A.W.H. Heijs, C. Lowe: *Phys. Rev. E*, 1995, vol. 51, pp. 4346-4352.
- [22] S. Ergun: *Chem. Engg. Prog.*, 1952, vol. 48, pp. 89-94.
- [23] D.G. Eskin, Suyitno, L. Katgerman: *Prog. Mater. Sci.*, 2004, vol. 49, pp. 629-711.
- [24] B. Magnin, L. Maenner, et al.: *Mater. Sci. Forum*, 1996, vol. 217-222, pp. 1209-1214.
- [25] A. Yamanaka, K. Nakajima, et al.: *Revue Metall.-Cahiers D Inf. Techn.*, 1992, vol. 89, pp. 627-633.
- [26] Y. Won, T. Yeo, et al.: *Metall. Mater. Trans. B*, 2000, vol. 31B, pp. 779-794.
- [27] A. Alankar, M. A. Wells: *Mater. Sci. Eng. A*, 2010, vol. 527, pp. 7812-7820.
- [28] A. B. Phillion, S. L. Cockcroft, P. D Lee: *Modell. Simul. Mater. Sci. Eng.*, 2009, vol. 17, pp. 1-15.
- [29] A. M. Glenn, S. P. Russo, P. J. K. Paterson: *Metall. Mater. Trans. A*, 2003, vol. 34A, pp. 1513-1523.
- [30] J. M. Drezet, M. Rappaz: TMS-Light Metals, J.L. Angier, ed., Warrendale, PA, 2001: 887-893.
- [31] H. Hao, D.M. Maijer, et al.: *Metall. Mater. Trans. A*, 2010, vol. 41A, pp. 2067-2077.
- [32] C. Monroe, C. Beckermann: *Mater. Sci. Eng. A*, 2005, vol. 413-414, pp. 30-36.

Figure Captions:

Fig. 1 Schematic of a DC cast billet showing the location of the mushy zone upon of interest in this work, along with the semi-solid microstructure (after Rappaz et al.^[15]) upon which the mass balance is performed. Solid deformation occurs in the directions of the x - and y -axes, as indicated.

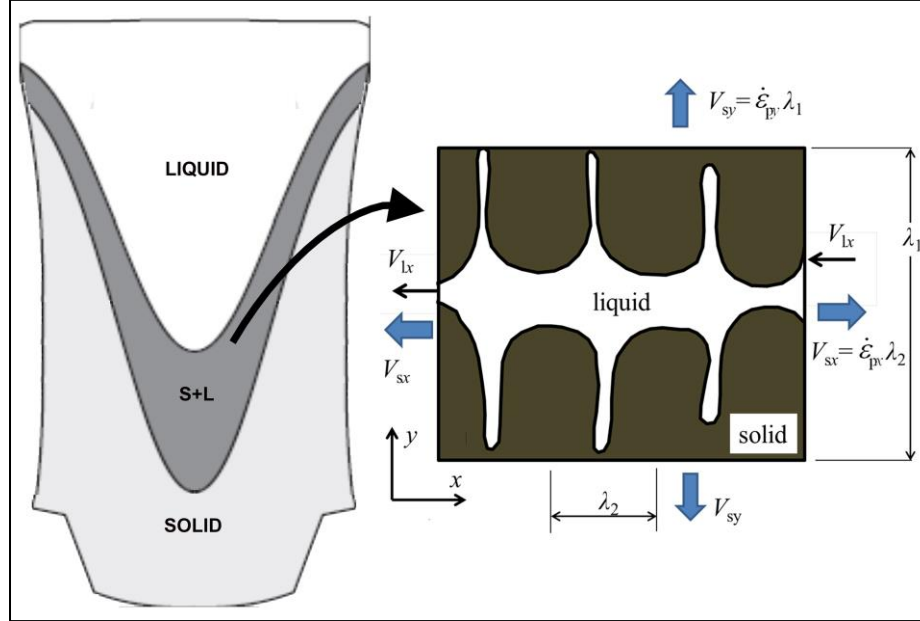


Fig. 2 Pore fraction vs. dimensionless Niyama criterion for an Al-3wt.%Cu alloy with an applied strain rate $\dot{\epsilon}_{py}$ of 10^{-3} s^{-1} .

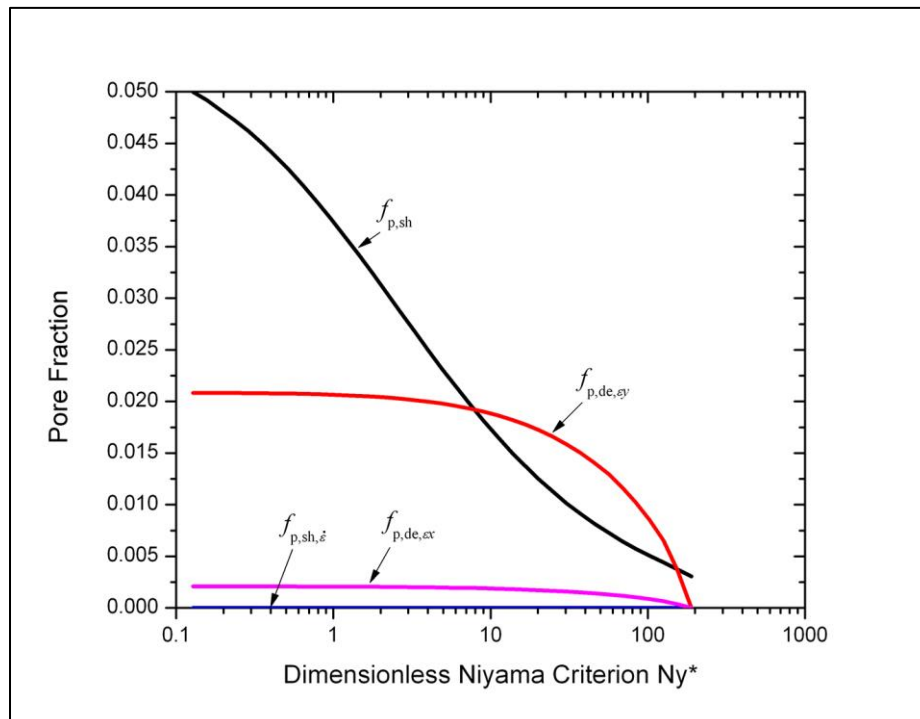


Fig. 3 Pore fraction vs. alloy composition for equal Niyama values, and an applied strain rate $\dot{\epsilon}_{pv}$ of 10^{-3} s^{-1} .

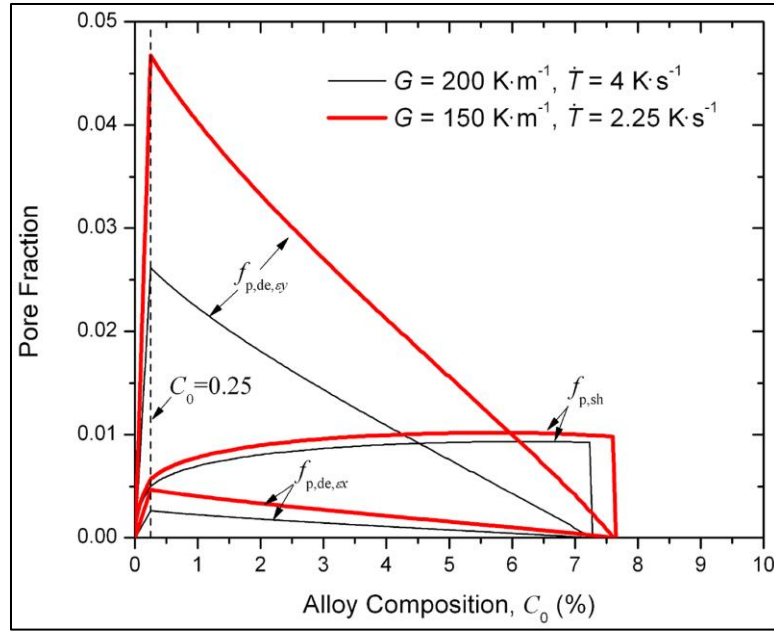


Fig. 4 Schematic of the axi-symmetric DC casting model showing the billet dimensions and placement of the boundary conditions (Γ_1 – Γ_5).^[13]

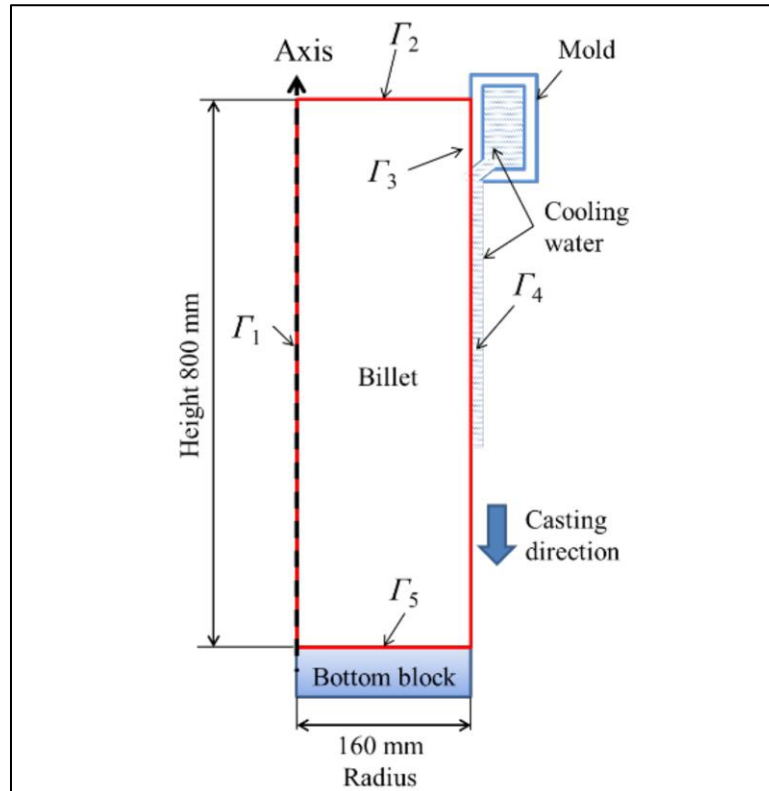


Fig. 5 Distribution of pore fractions and strain rate vs. distance from the bottom block at a casting speed $56 \text{ mm} \cdot \text{min}^{-1}$.

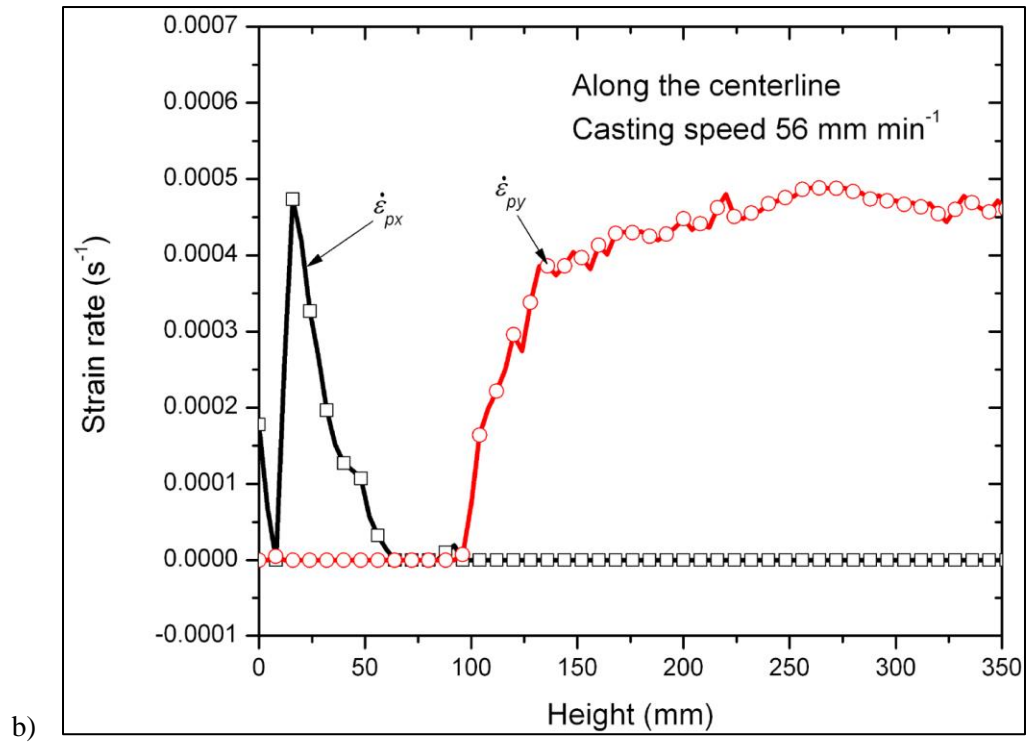
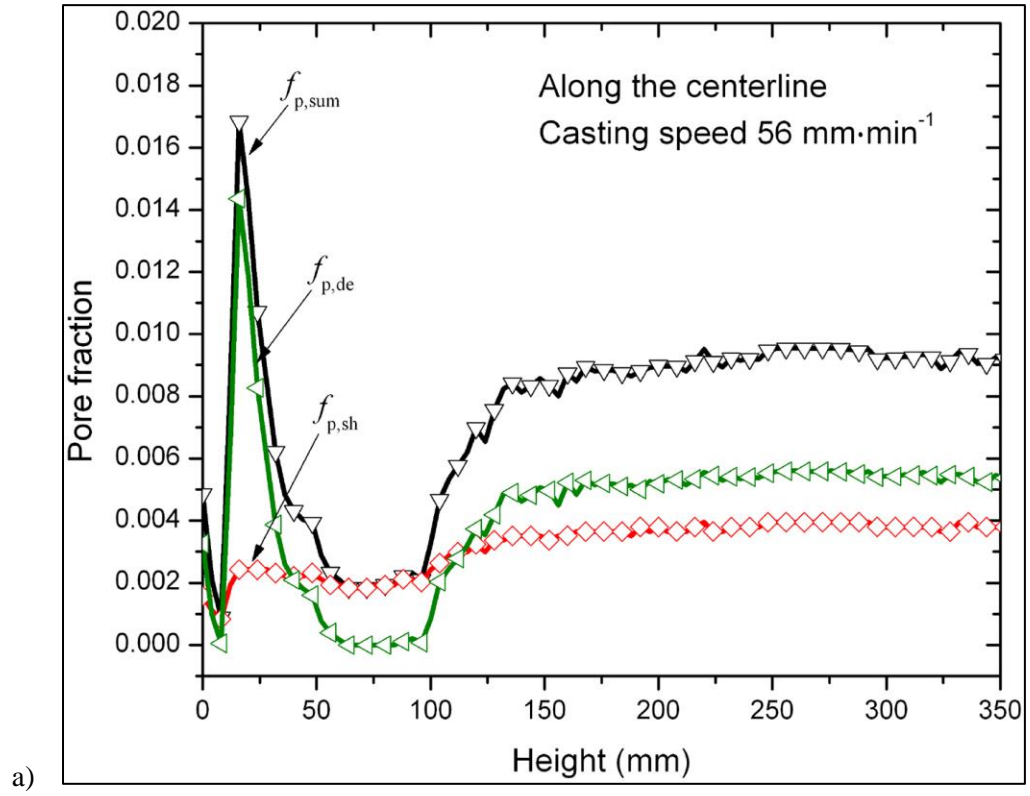


Fig. 6 Contour maps showing the variation of pore fractions (a) $f_{p, \text{sum}}$, (b) $f_{p, \text{de}}$ and critical liquid fraction (c) f_{cr} throughout the billet for a casting speed of $56 \text{ mm} \cdot \text{min}^{-1}$.

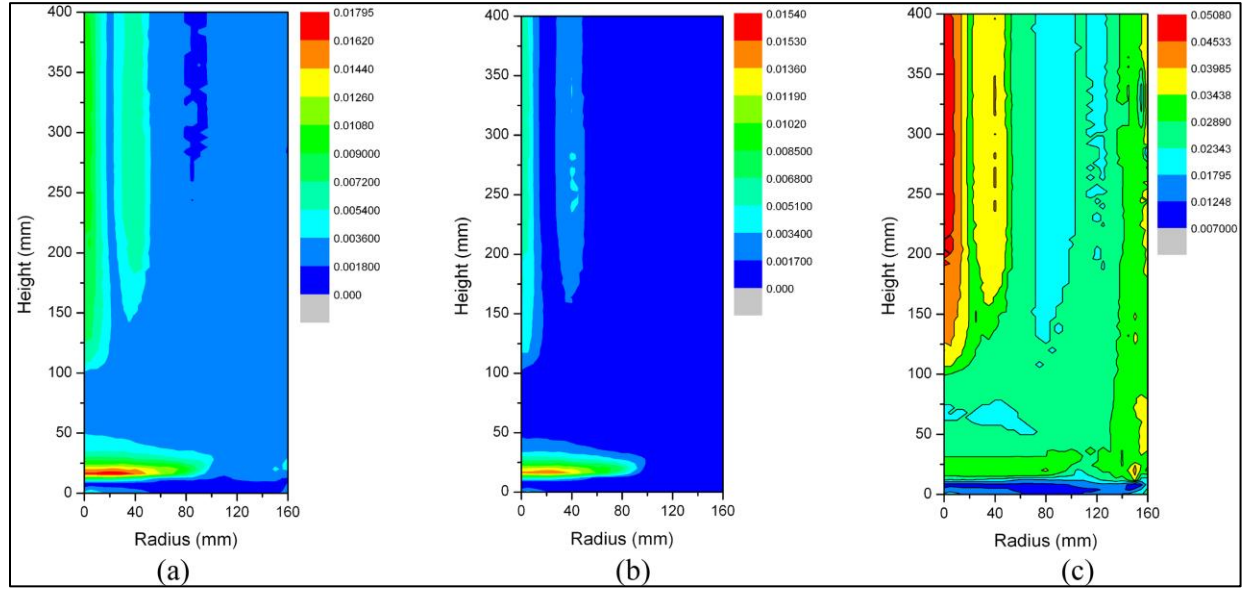


Fig. 7 Distribution of pore fractions (a) $f_{p,\text{sum}}$ and (b) $f_{p,\text{de}}$ along the centerline of the billet at different casting speeds.

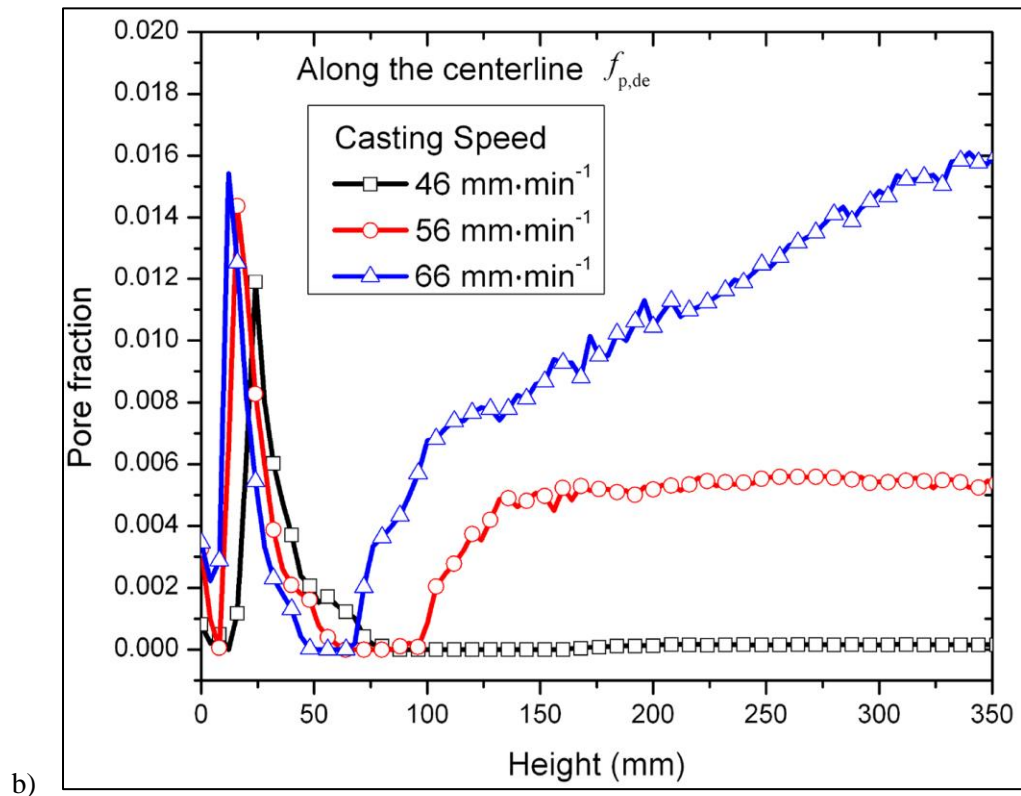
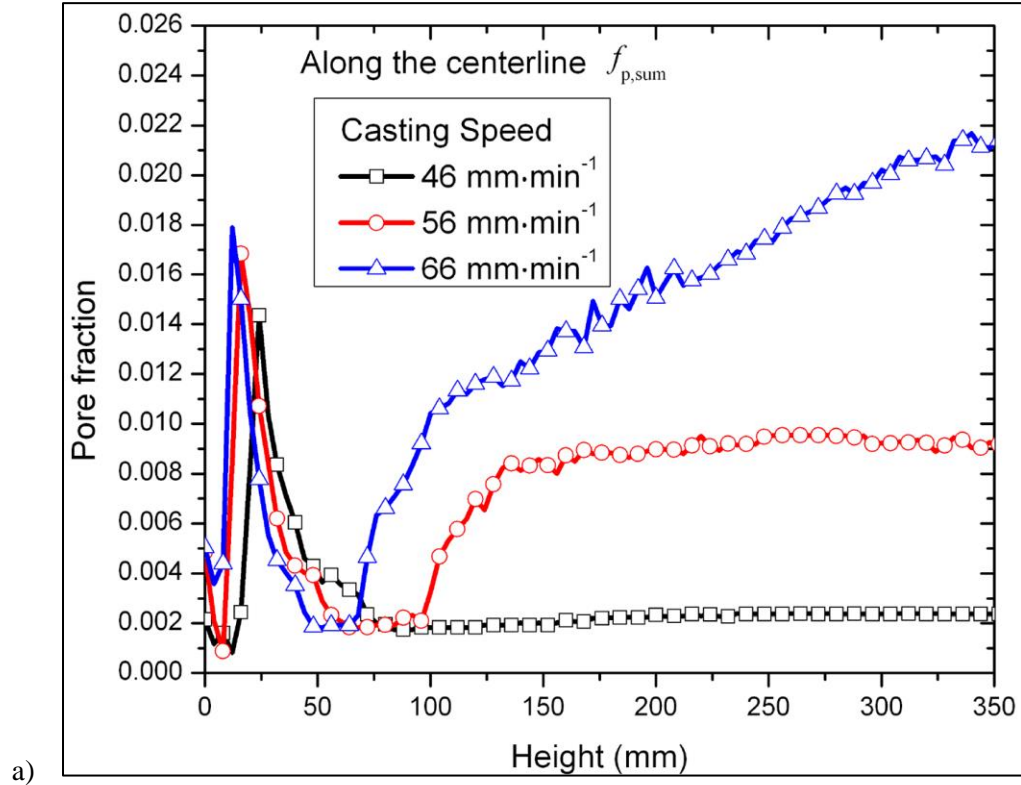


Fig. 8 Distribution of pore fractions (a) $f_{p,sum}$ and (b) $f_{p,de}$ along the radius of the billet at different casting speeds.

